International Journal of Environmental Science and Technology (2022) 19:11249–11262
https://doi.org/10.1007/s13762-022-04282-w

ORIGINAL PAPER

Cost-effective and sunlight-driven degradation of anionic and cationic dyes with pure ZnO nanoparticles

R. Stanley[1,3] · J. Alphas Jebasingh[2] · S. Manisha Vidyavathy[3]

Received: 9 December 2020 / Revised: 21 October 2021 / Accepted: 7 May 2022 / Published online: 4 June 2022

Abstract

In this study, economical, harmless and environmentally friendly zinc oxide (ZnO) nanoparticles (NPs) were synthesized by using the co-precipitation method. X-ray diffraction confirmed the presence of ZnO with a hexagonal structure. Scanning electron microscopy and energy-dispersive X-ray spectroscopy results revealed ZnO with plate- and chain-like structures and high elemental purity. UV–visible spectroscopy recorded an absorption peak at 422 nm. The visible region absorption facilitated an increased absorption of light energy from sunlight. The photocatalytic performance of the prepared ZnO NPs was calculated by the degradation of both cationic dyes, i.e. methylene blue (MB) and rhodamine B and anionic dye methyl orange under sunlight. The degradation and mineralization efficiencies of MB were 98.1% and 91.96%, respectively. Additionally, the ZnO photocatalyst was reused up to four times for the degradation of dyes. This work could create a new pathway for futuristic development of sunlight-driven degradation of anionic and cationic dyes with ZnO NPs and resolve the worldwide photocatalytic and wastewater remediation issues.

Graphical abstract

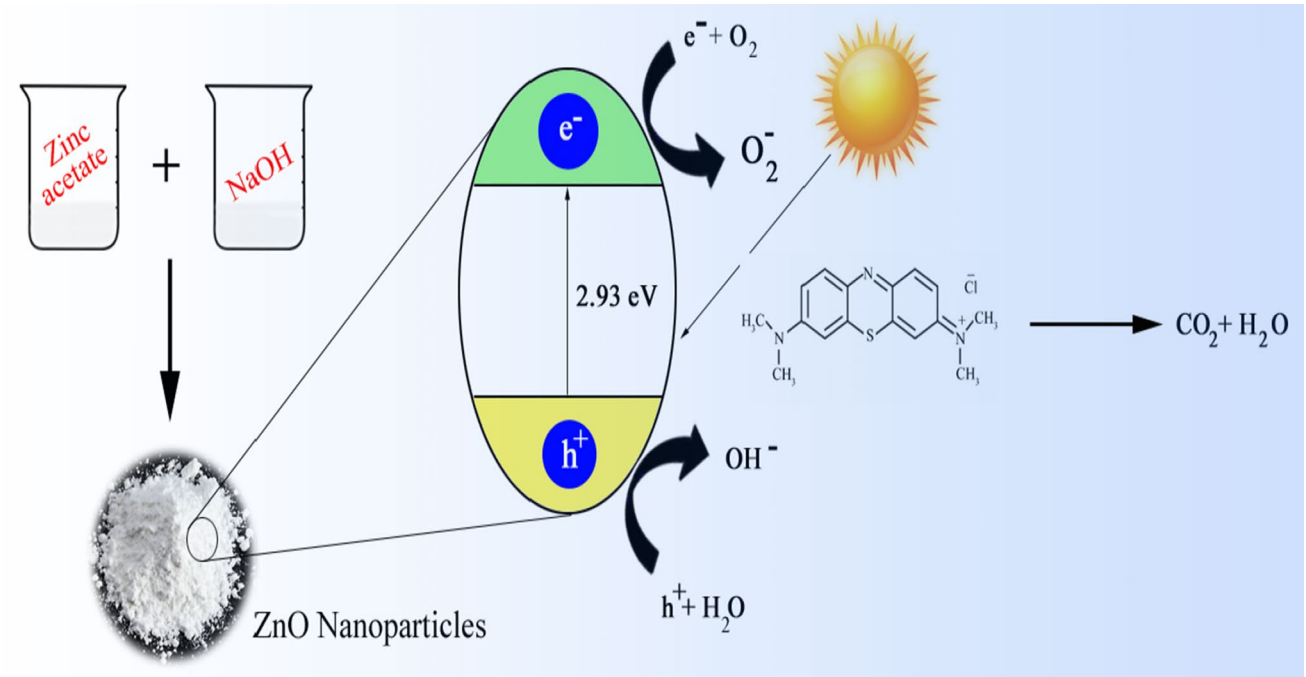

Editorial responsibility: Samareh Mirkia.

Extended author information available on the last page of the article

Keywords ZnO nanoparticles · Bandgap reduction · Methylene blue · Methyl orange · Sunlight photocatalysis · High degradation efficiency

Introduction

Today's world is more polluted than ever, because of egregious levels of contaminants present in air, water and food materials. This is due to the accumulation of industrial hazardous wastes in the environment. This turns the present world into a dangerous place for humans to live. Among all the other pollutants, water contaminants present in notable water have become a major threat towards the diurnal lives of human beings. Dyes and pigments released from textile, paper, leather, food and chemical industries are the primary sources of water contaminants (Brunekreef and Holgate 2002; Kantiani et al. 2010; Richardson and Ternes 2018). Even the presence of a minimum amount of dye (< 0.001 g/L) in drinking water causes severe problems to humanity (Song et al. 2015). Right now, researchers are focusing on treating water bodies in an economical and eco-friendly way, to neutralize water pollution without causing any damage to the environment. Among all the strategies, sunlight-based water treatment attracts more attention as it is freely available, sustainable, easy to access and environment-friendly.

Semiconductor-based photocatalysts are highly efficient, pollution-free, recyclable, green and low-cost materials to treat water contaminants using sunlight. The efficiency of the photocatalysts had limited realistic application because of insufficient visible light usage of the solar spectrum and fast recombination of charge carriers, thus altering the photocatalysis rate of dye degradation. Developing a highly efficient, photocatalytic material that could absorb photons from the solar spectrum on a large scale, and which could synthesize easily, and economically, is an onerous task. Many semiconductors are being used as photocatalysts (e.g. CdO, CeO_2, NiO, SiO_2, TiO2, ZnO, etc.), of which ZnO and TiO_2 are widely used in the degradation of organic pollutants in water (Jebasingh et al. 2019). Compared to TiO_2, ZnO has always been a better photocatalytic material because of its higher UV spectrum absorption rate, better sunlight absorption, longevity of induced charge carriers, quick electron transfer, non-toxicity, cost-effective and higher stability (Samadi et al. 2016).

The photocatalytic performance of ZnO nanoparticles is largely preferred due to their morphology and size. Researchers have reported ZnO nanoparticles, with different sizes and morphologies such as rice, custard apple, flower, nanopencils, spherical, flower with petals, rod and hexagonal. Out of the various methods available to produce ZnO NPs in large quantities (microwave irradiation, biosynthesis, solvothermal, ultrasonication, hydrothermal, chemical precipitation, sol–gel, combustion and wet chemical) (Sun et al. 2011; Hossain et al. 2015; Kaviya and Prasad 2015, 2016; Welderfael et al. 2016; Patil et al. 2016; Senthilraja et al. 2016; Jerlin Jose et al. 2017; Nagabhushana et al. 2017; Prasannalakshmi and Shanmugam 2017; Chidambaram et al. 2018), co-precipitation is the preferred method to prepare pure ZnO NPs as it is less time-consuming, inexpensive and produces high yields of nanoparticles.

Nowadays, in order to reduce cost and power consumption, sunlight is used for photocatalysis instead of artificial (manmade or UV) light sources. One of the important parameters for consideration while using sunlight is the efficiency of dye degradation and dye concentration to catalyst ratio. According to recent research, pure ZnO NPs are less efficient in the presence of sunlight (Qi et al. 2017). Further, the efficiency of ZnO primarily depends on the position of the conduction band and valance band, which directly affects the segregation and recombination of the photo-induced electrons and holes pair.

Dyes are used to colour products in industries. Basically, dyes are classified into three types, namely, anionic, cationic and nonionic dyes. MB and RhB are the common cationic dyes and MO is a common anionic dye. These dyes are commonly used in wood, paper, leather, silk, textile, plastics, cosmetics, paint, printing, scientific research, food and pharmaceutical industries. These pernicious colourants pose health problems to human beings in the form of skin and eye irritation, gene mutations, allergic dermatitis and sometimes even intestinal cancer due to its carcinogenic and mutagenic nature (Smith and John 2016; Nestmann et al. 1979; Horváthováet.al. 2012; World Health Organization International Agency for Research on Cancer 2015). Removing these three organic dyes from polluted water is considered to be one of the major environmental remediation works by the scientist community.

In this work, a novel one-step synthesis method was designed to fabricate pure ZnO NPs in the form of nanorod and chain-like structure. Till date, there has not been any research on ZnO NPs, to degrade these three organic pollutants (MB, MO and RhB), under sunlight. This work has achieved complete degradation of MB, MO and RhB dyes, under sunlight irradiation, by using synthesized ZnO NPs.

The photocatalytic mechanism of ZnO NPs is discussed in detail at the end.

Materials and methods

Chemicals used

ZnO nanoparticles were prepared by using the following chemical reagents, namely, zinc acetate dihydrate (Pure 98%, M/s MERCK, CAS no. 5970-45-6) (molecular weight: 214.49 g/mol), ammonia solution 25% (M/s MERCK, CAS no. 1336-21-6) (molecular weight: 17.03 g/mol), ethanol (Pure 99.9%, M/s Jiangsu Huaxi International Trade, China) and sodium hydroxide pellets (Pure 98%, M/s SRL, India CAS no. 1310-73-2) (molecular weight: 40 g/mol). Methylene blue (M/s MERCK, C.I.No. 52015) (molecular weight: 319.86 g/mol), rhodamine B (M/s, MERCK, C.I.No. 45170) (molecular weight: 479.02 g/mol) and methyl orange (M/S, MERCK, C.I.No. 13025) (molecular weight: 327.33 g/mol), on dyes with no further purification.

Preparation of ZnO nanoparticles

The nanophotocatalyst was prepared by using the co-precipitation method. 1 mol/L of $Zn(CH_3COO)_2{\cdot}2H_2O$ was dissolved in 100 mL of deionized water and stirred continuously for complete dissolution of the compound. 2 mol/L of NaOH was added dropwise to the above solution. During the above addition, 3 ml of 25% ammonia was also added and the solution was continuously stirred for 60 min at room temperature. The beaker was kept for 12 h (overnight) without any disturbance. After 12 h, the supernatant was removed and the final white colour precipitate was washed several times with a mixture of ethanol and water (9:1). The filtered white colour solid product was dried at 100 °C for one day and then heated at 800 °C for two hours to obtain ZnO nanoparticles.

Characterization

The elemental structure and nature of the prepared ZnO sample were analysed by using powder X-ray diffraction (Bruker D8 Discover), through Cu Kα radiation ($\lambda = 0.154$ nm), in the 2θ range of 10–90°. The nanophotocatalyst morphology was investigated by using a high-resolution scanning electron microscope (HR-SEM, FEI Quanta FEG 200). The sample was mounted on a gold platform by sputter coating for HR-SEM analysis at various magnifications. Elemental composition was determined using energy-dispersive X-ray spectroscopy (EDX) (FEI Quanta FEG 200). X-ray photoelectron spectroscopy (XPS) was used to analyse the chemical state of elements and also the elements present in the sample. Monochromatic Al Kα radiation (1486.7 eV) was used as the source and the instrument was operated at 15 kV (XPS-Omicron). Optical studies were performed by using a UV–visible spectrophotometer (Shimadzu UV-1800), in the range of 200–800 nm. The photoluminescence (PL) study was carried out by using a Spectro Fluorometer (JASCO FP-6300) and the excitation wavelength was 433 nm. Fourier-transform infrared spectroscopy (FTIR) study was conducted to find out the functional groups present in the sample using a spectrometer (JASCO FT/IR 4100), in the range of 400–4000 cm^{-1}. Total organic carbon analyser was used to identify the mineralization efficiency of the dyes (Shimadzu TOC-VLPH analyser).

Photocatalytic studies

Photocatalytic properties of the prepared nanoparticles were studied with MB dye by using the following procedure: 0.02–0.120 g of nanoparticles were dispersed in 100 mL aqueous solution of 0.01 g/L MB dye and stirred for 30 min in the dark to attain adsorption–desorption equilibrium (Raghavan et al. 2015; Jebasingh et al. 2020). No volatility of the solvent was observed during illumination and a sample, without light adsorption, was collected. Later, this solution was exposed to sunlight from 11 a.m. to 2 p.m. in the month of June and the intensity was 75,000 lx. At regular time intervals, 3 mL of the MB solution was withdrawn and the absorbance, at 661 nm wavelength, was recorded. The percentage of photodegradation efficiency of the MB dye was calculated by using Eq. (1) (Stanley et al. 2019).

$$\%\ \text{of photodegradation of the dye}\ (\eta\%) = \left(\frac{C_o - C_t}{C_o}\right) \times 100 \tag{1}$$

where C_o is the initial concentration and C_t is the concentration at a selected time interval of the model dyes, respectively.

The same procedure was repeated for the MO and RhB dyes and the absorbance, at 463 nm for MO and 548 nm for RhB, was recorded.

The percentage of mineralization efficiency of the MB dye was calculated, by using Eq. (2).

$$\%\ \text{of Mineralization of the MB dye}\ (\eta\%) = \left(1 - \frac{\text{TOC}_t}{\text{TOC}_o}\right) \times 100 \tag{2}$$

where TOC_o denotes before the start of the photocatalytic reaction and TOC_t denotes after the photocatalytic irradiation, in the selected time interval.

Scavenger studies

Trapping experiment was done to find out the major and minor active species responsible for the photocatalytic degradation process by using different types of scavengers. For detection of the superoxide anion (O_2^-), hole (h_+) and hydroxyl radical ($^{\cdot}OH$) species, ascorbic acid (AA), ethylene diamine tetra acetic acid disodium salt dehydrate (EDTA) and isopropanol (IPA) scavengers were used, respectively (Stanley et al. 2021).

Results and discussion

Structural analysis

The powder XRD pattern of pure ZnO nanoparticles is shown in Fig. 1. ZnO diffraction peaks at 31.77°, 34.42°, 36.25°, 47.55°, 56.61°, 62.89°, 66.40°, 67.97°, 69.15°, 72.60°, 77.01° and 81.43° can be indexed to the (100), (002), (101), (102), (110), (103), (200), (112), (201), (004), (202) and (104) planes of the hexagonal wurtzite structure of ZnO nanoparticles and they are in accordance with the standard value of JCPDS (No. 36-1451, $a = 3.2498$, $c = 5.2066$, Space group-P63mc) (Li et al. 2014). There were no extra peaks present in this sample, which confirmed the high purity of synthesized ZnO nanoparticles.

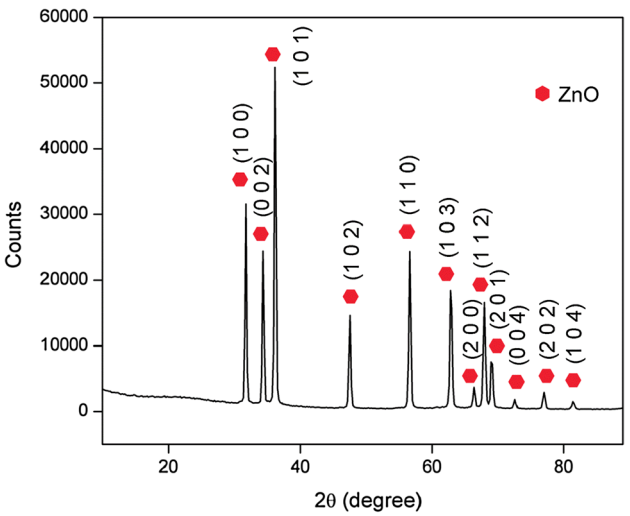

Fig. 1 The XRD pattern of the synthesized ZnO nanoplates

Average crystallite size was calculated by using the Debye–Scherer's equation Eq. (3). From the calculated values, the crystallite sizes of the ZnO nanoparticles were found to be in the range of 24–41 nm.

$$\text{Crystallite size } D\,(\text{nm}) = \frac{0.9\lambda}{\beta \cos\theta} \tag{3}$$

where D is the crystallite size of the synthesized particle (nm), λ is the wavelength of Cu Kα radiation (1.54 Å), β is the full-width half-maximum (FWHM), and θ is the Bragg's angle.

Morphology and elemental analysis

The morphology of the ZnO nanoparticles, prepared by using the co-precipitation method, is illustrated in Fig. 2a–d. The HR-SEM images indicate that the synthesized ZnO was a mixture of chain- and plate-like structures throughout the sample. The chain-like structure was arranged over the plate-like structure. Further, there was no agglomeration present in the sample. The size of the chain length and head varied from − 383 to − 674 nm and − 80 to − 290 nm, respectively. Nanoplates were arranged one over the other and their width and length varied from 210 to 419 nm and 320 nm to 1.57 µm, respectively. Particle size of ZnO was calculated by using the particle size analyser and it was found to be in the range of 70–800 nm and the maximum number of particles was present at 469 nm. Figure S1 displays the particle size analysis results of ZnO. The data were well matched with the HR-SEM images.

Additionally, EDX spectrum was analysed and results are displayed in Fig. 3. The EDX analysis yielded substantial evidence to the XRD results, which confirmed the purity of the synthesized ZnO NPs. Figure S2 exhibits the elemental mapping results of ZnO nanoparticles.

XPS analysis

Figure 4a presents the XPS survey spectrum of the synthesized ZnO NPs. XPS results revealed the chemical states of the elements and the surface chemical formation of the sample. XPS results confirmed the XRD and EDX results of the ZnO sample. Graphite tape was used in the sampling activity, which created the carbon peak in the spectrum. Peak at 283.78 eV indicated the presence of C 1s in the sample. C 1s was used to calibrate the other binding energies of the prepared sample. The high-resolution scans of Zn 2p, O 1s and C 1s are shown in Fig. 4b–d, respectively. The peaks at 1019.96 eV and 1044.12 eV corresponded to the Zn 2p region of 2p 1/2 and 2p 3/2 spin orbitals. Hence the oxidation state of Zn was + 2. Apart from Zn 2p region, the peaks at 9, 87 and 138 eV confirmed the presence of Zn 3d,

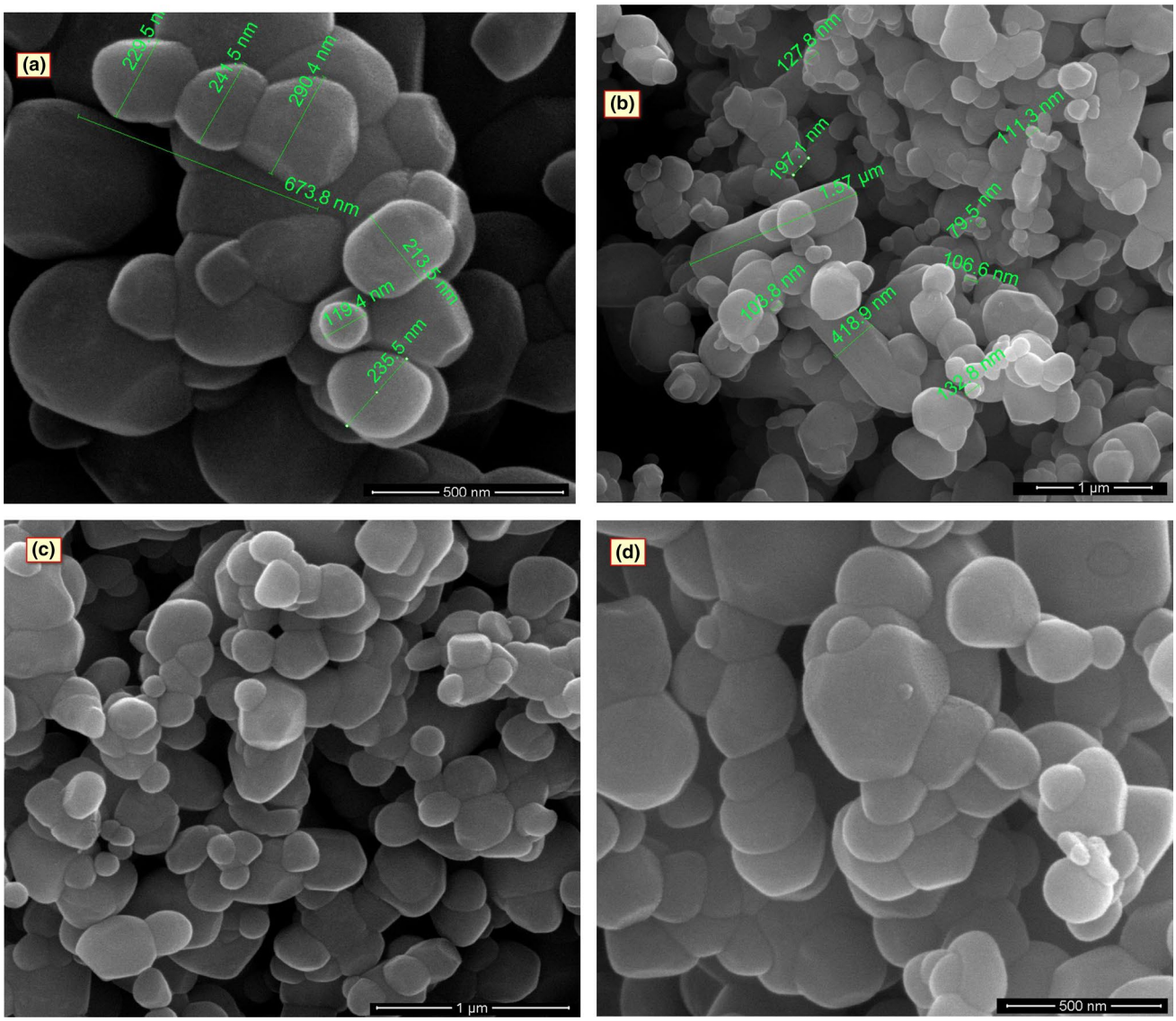

Fig. 2 The HR-SEM images of pure ZnO with different magnifications

3p and 3s spin orbitals, respectively (Kanjwal et al. 2015). The binding energy of 1072 eV indicated the presence of Na 1s in the ZnO NPs. The peak at 530.7 eV corresponded to the surface hydroxyl group present in the ZnO NPs. These hydroxyl groups promote the trapping of photoexcited electrons and holes, which improved the photodegradation efficiency of ZnO (Ansari et al. 2013).

FTIR analysis

The FTIR spectrum of the ZnO NPs, synthesized by using the co-precipitation method, is shown in Fig. 5. The band, present at 448 and 487 cm^{-1}, was due to the stretching vibrations of Zn–O in the ZnO sample (Amaranatha Reddy et al. 2015). The sharp and immense peaks at 1122 and 2358 cm^{-1} related to the C–O group and O=C=O vibration from the atmospheric air to the ZnO surface in the FTIR analysis (Mardani et al. 2015; Gharagozlou and Naghibi 2018). The broad peaks, at 1402, 1634, 3138 and 3405 cm^{-1}, were related to the stretching vibrations of O–H, caused by very low amount of water molecules present in the ZnO NPs. The above results confirmed the successful fabrication of the ZnO nanoparticles.

Optical analysis

In order to investigate the photon absorbance ability of ZnO NPs, the UV–visible spectroscopy analysis was carried out. Figure 6 depicts the UV–visible absorption spectrum of the

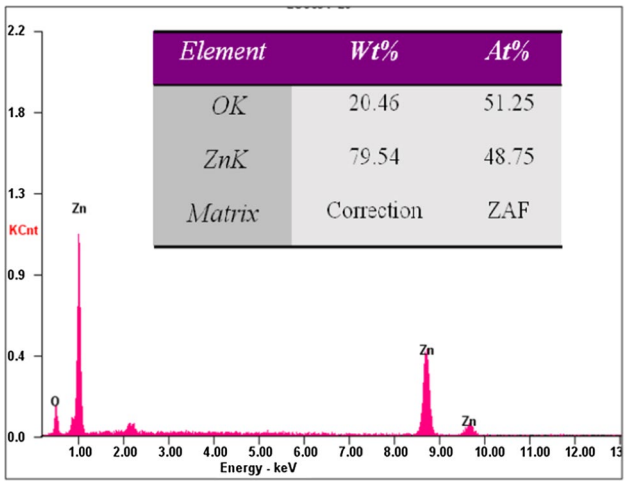

Fig. 3 The EDX spectrum of pure ZnO

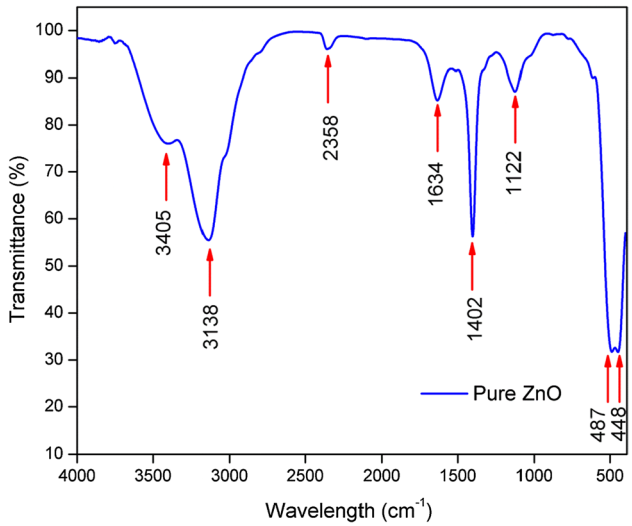

Fig. 5 FTIR spectrum of pure ZnO nanoplates

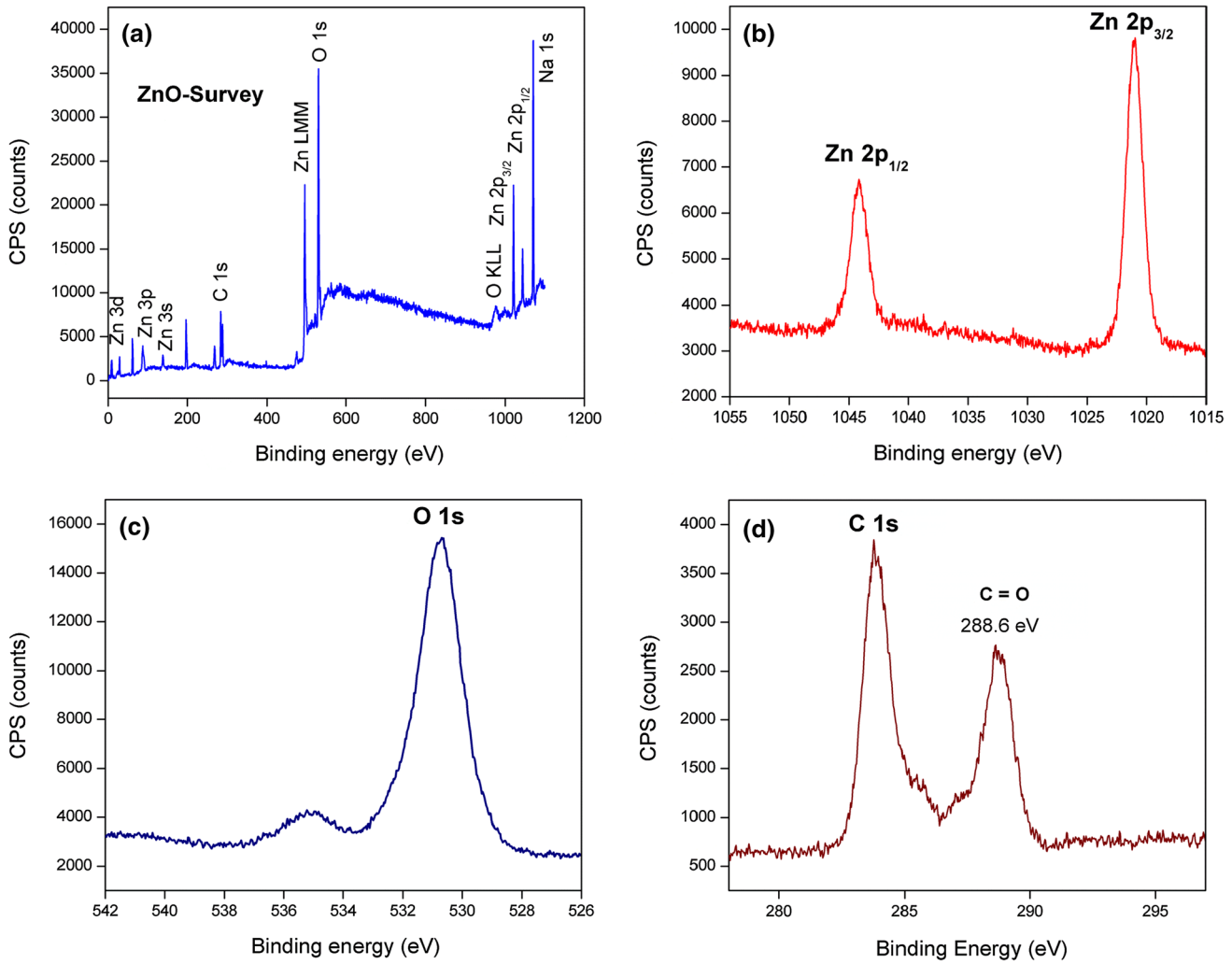

Fig. 4 **a** XPS survey spectra of ZnO NPs. **b–d** High-resolution scan of Zn 2p, O 1s and C 1s

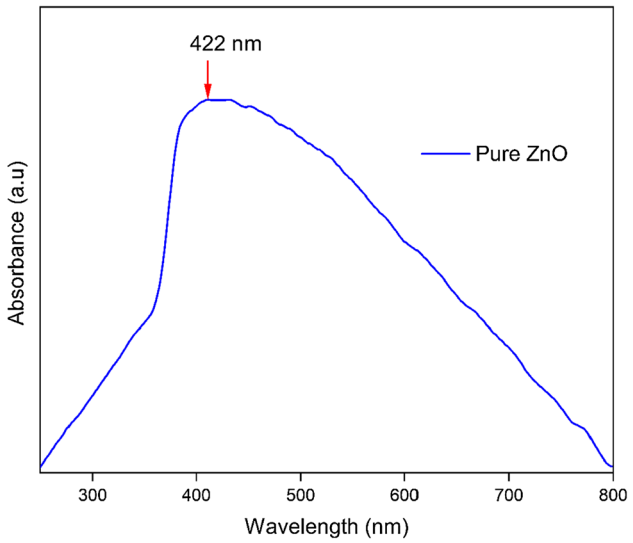

Fig. 6 UV–visible absorption spectra of the prepared ZnO photocatalyst

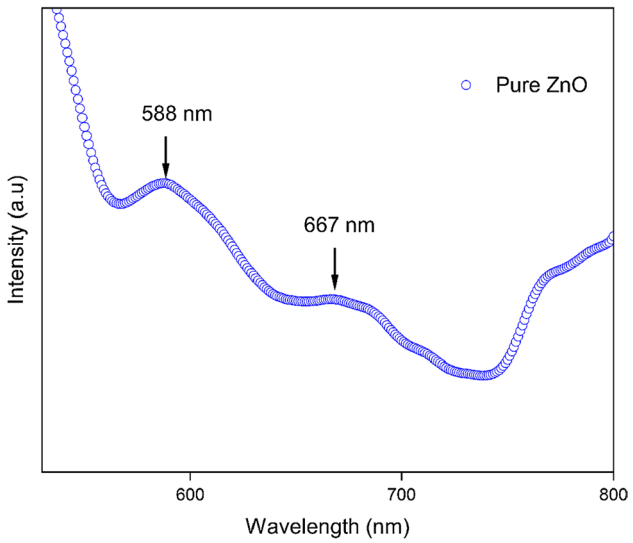

Fig. 7 Room temperature PL spectrum of pure ZnO NPs

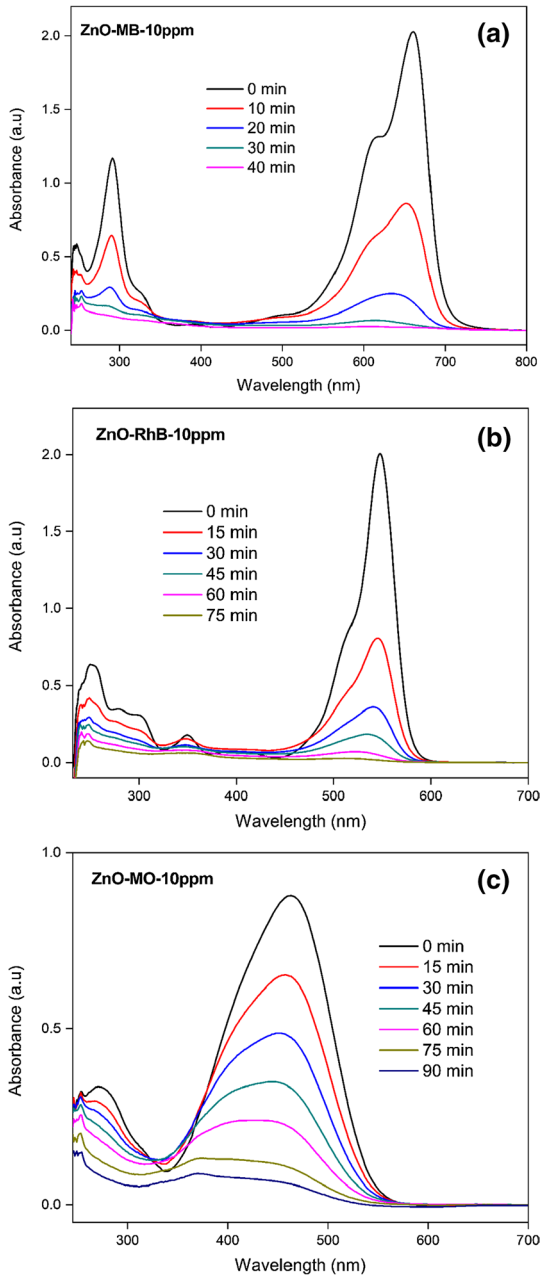

Fig. 8 Photocatalytic degradation of **a** MB, **b** RhB and **c** MO dyes by the prepared ZnO Nanoplates (dye concentration = 10 ppm; volume of dye = 100 ml)

synthesized ZnO NPs, which indicated the optical absorption in the visible region at 422 nm. The bandgap was calculated from Eq. (4) (Radhika and Thomas 2017).

$$E_g = 1239.8/\lambda \quad (4)$$

where E_g is energy bandgap (eV) and λ is the absorption wavelength (nm). The calculated optical bandgap energy is 2.93 eV (Choi et al. 2015). The bandgap decreased drastically when compared to ZnO previously reported (Kumar et al. 2018). Due to the modified co-precipitation method, the bandgap was greatly reduced, without any doped material or surfactant. Dominant bathochromic effect in the visible absorption region and narrow bandgap energy of ZnO

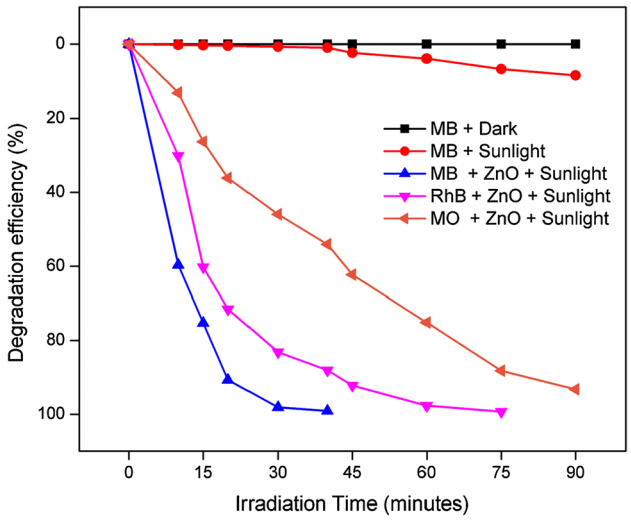

Fig. 9 Dye degradation efficiency of pure ZnO over MB, RhB and MO dyes

NPs provided the pathway to promote the usage of sunlight in an efficient manner. This ultimately increased the photocatalytic degradation efficiency of the synthesized ZnO NPs.

Photoluminescence analysis

Photoluminescence (PL) spectroscopy is an effective technique to investigate the efficiency of the trapped charge carriers, reunion of electron/hole pairs, defects and vacancies in the prepared sample. Figure 7 shows the PL emission spectrum of ZnO NPs, which displays bands at a wavelength of 588 nm, attributed to the yellow–orange emission and 667 nm, which corresponds to the red emission. Both the emission peaks were in the visible range. The intense yellow–red emission at 588 nm (2.1 eV) was related to the oxygen interstitials O_i, due to the band transfer of the zinc interstitial (Zn_i) to the oxygen interstitial (O_i) in the ZnO NPs (Alvi et al. 2011). The confined red emission at 667 nm (1.85 eV) corresponded to the oxygen vacancies (V_o). It is important to note that the surface defects, present in the ZnO NPs, were the reason for the life cycle of the photo-generated electron–hole pair. It automatically enhanced the photocatalytic degradation process (Budrugeac et al. 2011).

Photocatalytic degradation of anionic and cationic dyes

The photocatalytic activity against the pollutants present in water, by the metal oxide semiconductors, is essential for natural restoration. The photocatalytic degradation of MB, RhB and MO over the ZnO NPs was evaluated under sunlight irradiation. Figure 8 depicts the photodegradation, time-dependent UV–visible absorption spectra of the different dyes, degraded at different time intervals, by ZnO. For each dye, the photocatalyst amount varied from 20 to 120 mg, in order to optimize the dye degradation efficiency of the prepared ZnO. MB, RhB and MO dyes were degraded completely, with the use of 100, 120 and 100 mg of ZnO NPs, respectively. The initial MB absorption peak was at 661 nm and as the sunlight irradiation time increased, the peak shifted towards 600 nm. Finally, the 661 nm and 217 nm peaks disappeared completely. In other words, benzene rings present in the MB were achromatized and decomposed fully (Radhika and Thomas 2017). The initial absorption peak of MO was 463 nm and 271 nm. The 463 nm peak shifted towards 350 nm and the 271 nm peak was not visible after 90 min. The two emission bands of ZnO NPs came under the MB and RhB absorption region,

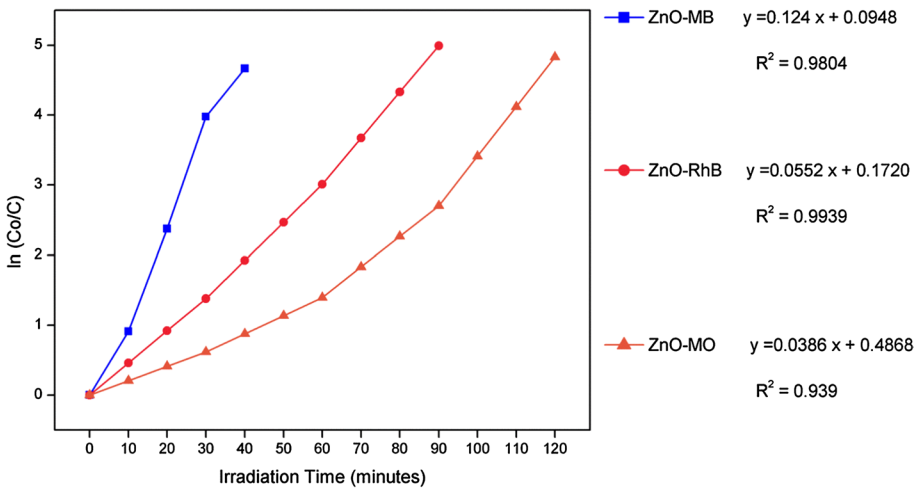

Fig. 10 Kinetic fitting curve of the degradation of MB, RhB and MO by ZnO NPs

Table 1 Degradation efficiency of ZnO towards the MB, RhB and MO dyes

Dye/Catalyst	20 mg	40 mg	60 mg	80 mg	100 mg	120 mg
MB—30 min	76.8	90.8	97	97.7	**98.1**	98
RhB—60 min	81.5	90	93.7	91.7	95.1	**97.7**
MO—90 min	40	72.2	86.4	91.9	**93.3**	89.2

which was the reason behind the efficient degradation of both the dyes, when compared to MO dye. The highest photocatalytic degradation efficiency of MB, RhB and MO dyes, over the prepared ZnO NPs, was 98.1%, 97.7% and 93.3%, respectively. The blank tests of self-degradation of the three organic dyes were conducted in sunlight and the removal rate of the dyes was very low (i.e.) for MB, 7.7% for 80 min; MO and RhB did not degrade under sunlight. The photodegradation efficiency of the ZnO NPs, over various organic dyes, is shown in Fig. 9.

In order to understand the reaction kinetics of degradation, the well-known Langmuir–Hinshelwood Model for degradation of organic pollutants was used. The results of our photocatalytic activity complied with the pseudo-first-order kinetics. Figure 10 shows the plots between ln (C_o/C) and sunlight irradiation time. The graph shows the linearity of the photocatalytic degradation of ZnO NPs against MB, MO and RhB dyes. The calculated rate constant K values were 0.1326, 0.0629 and 0.03 min^{-1} for MB, RhB and MO, respectively.

The degradation efficiency of ZnO nanorods on MB, RhB and MO dyes was reported after three hours of visible light irradiation, at 35.3%, 29.3% and 22.6% (Ranjith et al. 2017). Due to the fast recombination of phototriggered electron–hole pair charge carriers and wide bandgap of ZnO, the degradation efficiency was greatly reduced (Maya-Treviño et al. 2018). In this research work, one can find that these three organic dyes were degraded completely, under sunlight, by ZnO NPs. The dye degradation efficiency was greatly influenced by the bandgap reduction of ZnO, as this allowed the ZnO NPs to absorb more visible light photons from sunlight. Large numbers of electrons were excited from the valence band to the conduction band, in the ZnO surface. The holes created in the valence band reacted with the oxygen present in the water substance and produced the $OH^{\bullet}$ radicals. The energized electrons reacted with the O_2 and formed the $O_2^{\cdot-}$ radicals. Both $OH^{\bullet}$ and $O_2^{\bullet-}$ radicals were powerful oxidizing agents, responsible for the degradation of organic dyes.

Effect of catalyst dosage

In order to optimize the catalyst amount for the degradation of dyes, ZnO nanoparticles were taken from 20 to 120 mg,

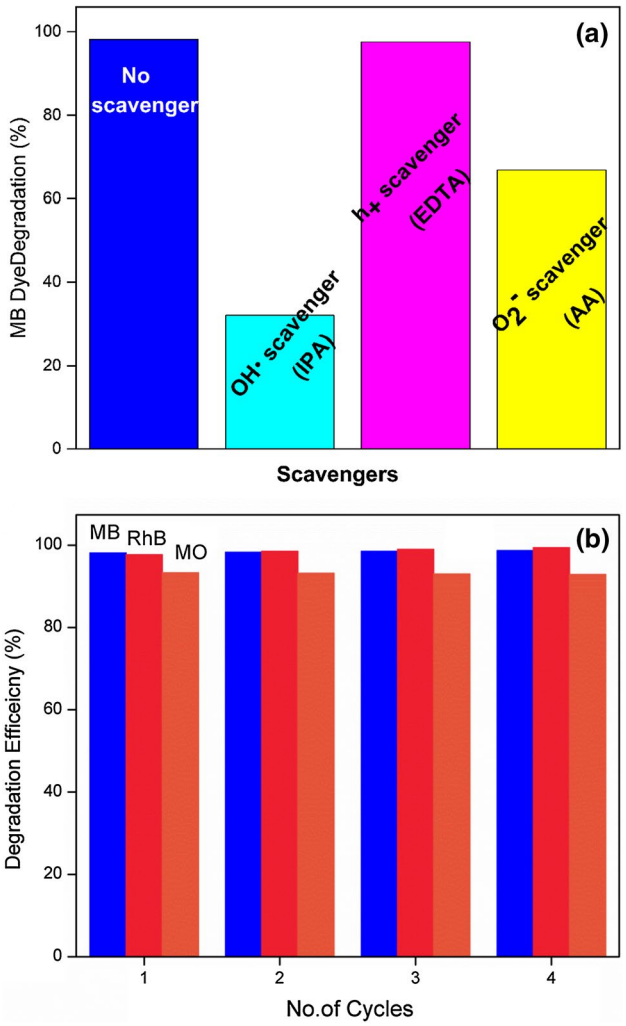

Fig. 11 Effect of scavengers over the MB dye by ZnO NPs (**a**) and ZnO NPs recycling test for MB, RhB and MO dyes (**b**)

Table 2 Comparison of various parameters of our synthesized ZnO NPs with other recent ZnO-based studies

Material	Dye	Dye (mg/L)	Catalyst (mg)	Light source	Dye degradation (%)	Time for degradation (min)	Ref.
ZnO	MB	40	100	Sunlight	50	240	Sun et al. (2011)
ZnO	MB	0.02×10^{-3} M	500	Sunlight	≈ 60	90	Kaviya and Prasad (2015)
ZnO	MB	7.9×10^{-4} M	130	Sunlight	90	120	Hossain et al. (2015)
ZnO	MB	0.02×10^{-3} M	700	Sunlight	≈ 92	90	Kaviya and Prasad (2016)
ZnO	MB	3×10^{-4} M	2000	Sunlight	89.1	60	Senthilraja et al. (2016)
ZnO	MB	10	10	Sunlight	≈ 83	90	Patil et al. (2016)
ZnO	MB	20	200	Sunlight	68.6	135	(Welderfael et al. (2016)
ZnO	MB	1	2000	Sunlight	≈ 100	75	Prasannalakshmi and Shanmugam (2017)
ZnO	MB	20	40	Sunlight	40	60	Nagabhushana et al. (2017)
ZnO	MB	30	100	Sunlight	≈ 65	50	(Radhika and Thomas 2017)
ZnO	MB	10	50	Sunlight	35.3	120	Ranjith et al. (2017)
ZnO	MB	10	100	Sunlight	98.1	30	This work

Table 3 Comparative study on the photocatalytic degradation of MO dye by ZnO NPs

Material	Dye	Dye (mg/L)	Catalyst (mg)	Light source	Dye degradation (%)	Time for degradation (min)	Ref.
ZnO	MO	10	100	Sunlight	≈ 25	480	Nezamzadeh-Ejhieh and Moazzeni (2013)
ZnO	MO	10	N/A	Sunlight	≈ 25	150	Ptasińska et al. (2016)
ZnO	MO	10	60	Sunlight	83	240	Yu et al. (2019)
ZnO	MO	10	5	Sunlight	≈ 15	360	Chang et al. (2016)
ZnO	MO	20	25	Sunlight	≈ 58	360	Hao et al. (2016)
ZnO	MO	10	100	Sunlight	93.3	90	This work

Table 4 Comparison of photocatalytic activity of ZnO over RhB dye in this work and recent literature

Material	Dye	Dye (mg/L)	Catalyst (mg)	Light Source	Dye degradation (%)	Time for degradation (min)	Ref.
ZnO	RhB	1×10^{-5} M	150	Sunlight	≈ 50	90	Ding et al. (2018)
ZnO	RhB	35	576	Sunlight	98	120	Print et al. (2017)
ZnO	RhB	5×10^{-5} M	50	Sunlight	≈ 45	45	Meshram et al. (2016)
ZnO	RhB	20	60	Sunlight	≈ 60	60	Chandrasekhar et al. (2015)
ZnO	RhB	5×10^{-6}	250	Sunlight	≈ 82	120	Abed et al. (2015)
ZnO	RhB	15	30	Sunlight	≈ 25	120	Ahmad et al. (2015)
ZnO	RhB	1×10^{-5} M	10	Sunlight	≈ 35	30	Yang et al. (2014)
ZnO	RhB	10	10	Sunlight	≈ 80	150	Neelgund et al. (2014)
ZnO	RhB	1×10^{-5} M	15	Sunlight	≈ 48	150	Wang et al. (2014)
ZnO	RhB	10	120	Sunlight	97.7	60	This work

for the dye concentration of 10 ppm, for both anionic and cationic dyes. Figures S3, S4 and S5 show the relationship between the C/C_0 and the sunlight irradiation time taken for the degradation of various dyes. Table 1 shows the degradation efficiency of ZnO photocatalyst, for the MB, RhB and MO dyes. For the cationic MO dye, 20 mg photocatalyst showed a very low degradation efficiency compared to other high amounts of photocatalyst. This was due to the less number of active sites created in the ZnO photocatalyst and this induced the formation of less number of hydroxyl radicals, leading to the lower degradation efficiencies.

Active species detection

The trapping experiment was conducted to find out the photocatalytic mechanism and also the major and minor active species involved in the photocatalytic degradation of dyes. Figure 11a shows the different scavengers' efficiencies for the MB dye. The degradation efficiencies for AA, EDTA and IPA scavengers were 32%, 97.6% and 66.8%, respectively. In other words, O_2^- and $OH^\bullet$ radicals were the main active species for the degradation of MB dye. EDTA recorded a higher efficiency and it revealed that holes did not play any role in the degradation process. Based upon the trapping test results, the plausible photocatalytic mechanism of ZnO NPs, for the MB dye, under natural solar radiation, is shown in Eqs. (5) to (10).

$$\mathrm{ZnO} + \text{sunlight} \rightarrow \mathrm{ZnO}\left(e_{cb}^- + h_{vb}^+\right) \quad (5)$$

$$e_{cb}^- + O_2 \rightarrow O_2^{\cdot -} \quad (6)$$

$$\mathrm{MB} + O_2^{\cdot -} \rightarrow CO_2 + H_2O \quad (7)$$

$$h_{vb}^+ + H_2O \rightarrow \mathrm{ZnO} + H^+ + OH^- \quad (8)$$

$$h_{vb}^+ + OH^- \rightarrow OH^{\cdot} \quad (9)$$

$$\mathrm{MB} + OH^{\cdot} \rightarrow CO_2 + H_2O. \quad (10)$$

Tables 2, 3 and 4 display the excellent photocatalytic activity of synthesized ZnO NPs, over MB and MO dyes, as compared to the ZnO from recent literature. In short, the above results revealed the highest degradation efficiency over organic pollutants, under sunlight. For the MB dye, after 210 min of sunlight irradiation the mineralization efficiency was determined to be 91.96% by using the TOC analysis.

Reusability of ZnO

In addition, the reusability of the prepared ZnO NPs over the different anionic and cationic dyes was analysed. Figure 11b shows the reproducibility of the ZnO sample over different dyes. First time used ZnO nanoparticles were cleaned with water multiple times, then filtered and heat treated at 80 °C for couple of hours. Then, the dried sample will be used for the second time and the same procedure will be followed for the consecutive recycling test. After four times of recycling, the photocatalytic degradation efficiency is 98.7%, 99.4% and 92.9% for MB, RhB and MO dyes, respectively. This suggests that, after recycling multiple times the degradation efficiency did not reduce much compared to the first time. So, the prepared ZnO NPs can be very useful in the wastewater treatment for multiple use.

Conclusion

A novel ZnO NPs, which was cost-effective, high purity and eco-friendly, was fabricated. The hexagonal structure of ZnO was confirmed by the XRD analysis. The presence of the combination of plate- and chain-like morphologies throughout the samples was observed by using HR-SEM. Elemental purity was confirmed by XRD and EDX data. The prepared ZnO degraded the MB, RhB and MO dyes completely under sunlight irradiation at a lesser time interval when compared to that reported in the recent literature. The mineralization efficiency of the MB dye was 91.96%. The absorption band and the emission spectrum of ZnO NPs, in the visible region, led to an increased photocatalytic degradation of organic dyes. Bandgap of ZnO was greatly reduced by this novel synthesis method, which induced the reduction of the recombination of electron–hole pairs in the ZnO NPs. O_2^- and $OH^{\cdot}$ radicals were the active species responsible for the photocatalytic degradation of MB dye. The reusability of ZnO was tested four times, without any change in the degradation efficiency. From the above results, a plausible photocatalytic mechanism was proposed. This would create a new paradigm in the photocatalytic degradation of dyes and wastewater remediation.

Supplementary Information The online version contains supplementary material available at https://doi.org/10.1007/s13762-022-04282-w.

Acknowledgements The authors thank the Anna Centenary Research Fellowship (ACRF) (Grant No: CFR/ACRF/2015/27) Anna University, Chennai, India, for giving financial assistance to do this study. The authors extend thanks to Dr. S. Sivanesan, Professor, DAST, Anna

University, for providing the UV–visible spectrometer, IIT Madras SAIF & Chemistry, MNIT-MRC-Jaipur, for providing the analytical support.

Declarations

Conflict of interest The authors declare that they have no conflict of interest.

Ethical approval This article does not contain any studies with human participants or animals performed by any of the authors.

References

Abed C, Bouzidi C, Elhouichet H et al (2015) Mg doping induced high structural quality of sol-gel ZnO nanocrystals: application in photocatalysis. Appl Surf Sci 349:855–863. https://doi.org/10.1016/j.apsusc.2015.05.078

Ahmad M, Ahmed E, Zafar F et al (2015) Enhanced photocatalytic activity of Ce-doped ZnO nanopowders synthesized by combustion method. J Rare Earths 33:255–262. https://doi.org/10.1016/S1002-0721(14)60412-9

Alvi NH, ul Hasan K, Nur O, Willander M (2011) The origin of the red emission in n-zno nanotubes/p-gan white light emitting diodes. Nanoscale Res Lett 6:130. https://doi.org/10.1186/1556-276X-6-130

Amaranatha Reddy D, Ma R, Kim TK (2015) Efficient photocatalytic degradation of methylene blue by heterostructured ZnO-RGO/RuO2 nanocomposite under the simulated sunlight irradiation. Ceram Int 41:6999–7009. https://doi.org/10.1016/j.ceramint.2015.01.155

Ansari SA, Khan MM, Ansari MO et al (2013) Biogenic synthesis, photocatalytic, and photoelectrochemical performance of Ag – ZnO nanocomposite. J Phys Chem C. https://doi.org/10.1021/jp410063p

Brunekreef B, Holgate ST (2002) Air pollution and health. Lancet 360:1233–1242. https://doi.org/10.1016/S0140-6736(02)11274-8

Budrugeac P, Calderón-Moreno JM, Carp O et al (2011) A green chemical approach to the synthesis of photoluminescent ZnO hollow spheres with enhanced photocatalytic properties. J Solid State Chem 186:17–22. https://doi.org/10.1016/j.jssc.2011.11.024

Chandrasekhar M, Nagabhushana H, Vidya YS et al (2015) Synthesis of Eu3+-activated ZnO superstructures: photoluminescence, judd-ofelt analysis and sunlight photocatalytic properties. J Mol Catal A Chem 409:26–41. https://doi.org/10.1016/j.molcata.2015.08.002

Chang X, Li Z, Zhai X et al (2016) Efficient synthesis of sunlight-driven ZnO-based heterogeneous photocatalysts. Mater Des 98:324–332. https://doi.org/10.1016/j.matdes.2016.03.027

Chidambaram S, Vijay A, Kumar GM et al (2018) Three-dimensional (3D) flower-like nanoarchitectures of ZnO-Au on MWCNTs for visible light photocatalytic applications. Appl Surf Sci 449:631–637. https://doi.org/10.1016/j.apsusc.2017.11.236

Choi YI, Jung HJ, Shin WG, Sohn Y (2015) Band gap-engineered ZnO and Ag/ZnO by ball-milling method and their photocatalytic and fenton-like photocatalytic activities. Appl Surf Sci 356:615–625. https://doi.org/10.1016/j.apsusc.2015.08.118

Ding F, Liu T, Chen C et al (2018) Low-temperature construction of MoS2 quantum dots/ZnO spheres and their photocatalytic activity under natural sunlight. J Colloid Interface Sci 530:714–724. https://doi.org/10.1016/j.jcis.2018.07.015

Gharagozlou M, Naghibi S (2018) Sensitization of ZnO nanoparticles by metal–free phthalocyanine. J Lumin 196:64–68. https://doi.org/10.1016/j.jlumin.2017.12.020

Hao C, Yang Y, Shen Y et al (2016) Liquid phase-based ultrasonic-assisted synthesis of G-ZnO nanocomposites and its sunlight photocatalytic activity. Mater Des 89:864–871. https://doi.org/10.1016/j.matdes.2015.10.041

Horváthová E, Kozics K, Srančíková A et al (2012) Borneol administration protects primary rat hepatocytes against exogenous oxidative DNA damage. Mutagenesis 27:581–588. https://doi.org/10.1093/mutage/ges023

Hossain MM, Ku BC, Hahn JR (2015) Synthesis of an efficient white-light photocatalyst composite of graphene and ZnO nanoparticles: application to methylene blue dye decomposition. Appl Surf Sci 354:55–65. https://doi.org/10.1016/j.apsusc.2015.01.191

Jebasingh JA, Stanley R, Manisha Vidyavathy S (2019) Low temperature titania nano particles for high performance solar photo degradation. Optik (stuttg) 179:901–908. https://doi.org/10.1016/j.ijleo.2018.09.164

Jebasingh JA, Stanley R, Manisha Vidyavathy S (2020) Sol-gel preparation of surfactants assisted titania for solar photocatalysis. Mater Lett 279:128460. https://doi.org/10.1016/j.matlet.2020.128460

Jerlin Jose Y, Manjunathan M, Joseph Selvaraj S (2017) Highly photocatalyst efficient in LEDs/solar active and reusable: Sm–ZnO–Ag nanoparticles for methylene blue degradation. J Nanostructure Chem 7:259–271. https://doi.org/10.1007/s40097-017-0236-3

Kanjwal MA, Chronakis IS, Barakat NAM (2015) Electrospun NiO, ZnO and composite NiO – ZnO nanofibers/photocatalytic degradation of dairy effluent. Ceram Int 41:12229–12236. https://doi.org/10.1016/j.ceramint.2015.06.045

Kantiani L, Llorca M, Sanchís J et al (2010) Emerging food contaminants: a review. Anal Bioanal Chem 398:2413–2427. https://doi.org/10.1007/s00216-010-3944-9

Kaviya S, Prasad E (2015) Biogenic synthesis of ZnO-Ag nano custard apples for efficient photocatalytic degradation of methylene blue by sunlight irradiation. RSC Adv 5:17179–17185. https://doi.org/10.1039/c4ra15293j

Kaviya S, Prasad E (2016) Eco-friendly synthesis of ZnO nanopencils in aqueous medium: a study of photocatalytic degradation of methylene blue under direct sunlight. RSC Adv 6:33821–33827. https://doi.org/10.1039/c6ra04306b

Kumar S, Dhiman A, Sudhagar P, Krishnan V (2018) ZnO-graphene quantum dots heterojunctions for natural sunlight-driven photocatalytic environmental remediation. Appl Surf Sci 447:802–815. https://doi.org/10.1016/j.apsusc.2018.04.045

Li SQ, Zhou PJ, Zhang WS et al (2014) Effective photocatalytic decolorization of methylene blue utilizing ZnO/rectorite nanocomposite

under simulated solar irradiation. J Alloys Compd 616:227–234. https://doi.org/10.1016/j.jallcom.2014.07.102

Mardani HR, Forouzani M, Ziari M, Biparva P (2015) Visible light photo-degradation of methylene blue over Fe or Cu promoted ZnO nanoparticles. Spectrochim Acta Part A Mol Biomol Spectrosc 141:27–33. https://doi.org/10.1016/j.saa.2015.01.034

Maya-Treviño ML, Guzmán-Mar JL, Hinojosa-Reyes L, Hernández-Ramírez A (2018) Synthesis and photocatalytic activity of ZnO-CuPc for methylene blue and potassium cyanide degradation. Mater Sci Semicond Process 77:74–82. https://doi.org/10.1016/j.mssp.2017.12.005

Meshram SP, Adhyapak PV, Amalnerkar DP, Mulla IS (2016) Cu doped ZnO microballs as effective sunlight driven photocatalyst. Ceram Int 42:7482–7489. https://doi.org/10.1016/j.ceramint.2016.01.154

Nagabhushana H, Renuka L, Nagaswarupa HP et al (2017) Synthesis of sunlight driven ZnO/CuO nanocomposite: characterization, optical, electrochemical and photocatalytic studies. Mater Today Proc 4:11782–11790. https://doi.org/10.1016/j.matpr.2017.09.095

Neelgund GM, Oki A, Luo Z (2014) ZnO and cobalt phthalocyanine hybridized graphene: Efficient photocatalysts for degradation of rhodamine B. J Colloid Interface Sci 430:257–264. https://doi.org/10.1016/j.jcis.2014.04.053

Nestmann ER, Douglas GR, Matula TI et al (1979) Mutagenic activity of rhodamine dyes and their impurities as detected by mutation induction in salmonella and DNA damage in chinese hamster ovary cells. Cancer Res 39:4412–4417

Nezamzadeh-Ejhieh A, Moazzeni N (2013) Sunlight photodecolorization of a mixture of methyl orange and bromocresol green by CuS incorporated in a clinoptilolite zeolite as a heterogeneous catalyst. J Ind Eng Chem 19:1433–1442. https://doi.org/10.1016/j.jiec.2013.01.006

Patil SS, Mali MG, Tamboli MS et al (2016) Green approach for hierarchical nanostructured Ag-ZnO and their photocatalytic performance under sunlight. Catal Today 260:126–134. https://doi.org/10.1016/j.cattod.2015.06.004

Prasannalakshmi P, Shanmugam N (2017) Fabrication of TiO2/ZnO nanocomposites for solar energy driven photocatalysis. Mater Sci Semicond Process 61:114–124. https://doi.org/10.1016/j.mssp.2017.01.008

Print I, Pm P, Mn A (2017) High degradation efficiency of organic dyes under sunlight irradiation for ZnO nanorods. Chem Technol Indian J 11:1–5

Ptasińska S, Zhang X, Dramićanin MD et al (2016) Enhanced photocatalytic degradation of methylene blue and methyl orange by ZnO: Eu nanoparticles. Appl Catal B Environ 203:740–752. https://doi.org/10.1016/j.apcatb.2016.10.063

Qi K, Cheng B, Yu J, Ho W (2017) Review on the improvement of the photocatalytic and antibacterial activities of ZnO. J Alloys Compd 727:792–820. https://doi.org/10.1016/j.jallcom.2017.08.142

Radhika S, Thomas J (2017) Solar light driven photocatalytic degradation of organic pollutants using ZnO nanorods coupled with photosensitive molecules. J Environ Chem Eng 5:4239–4250. https://doi.org/10.1016/j.jece.2017.08.013

Raghavan N, Thangavel S, Venugopal G (2015) Enhanced photocatalytic degradation of methylene blue by reduced graphene-oxide/titanium dioxide/zinc oxide ternary nanocomposites. Mater Sci Semicond Process 30:321–329. https://doi.org/10.1016/j.mssp.2014.09.019

Ranjith KS, Manivel P, Rajendrakumar RT, Uyar T (2017) Multifunctional ZnO nanorod-reduced graphene oxide hybrids nanocomposites for effective water remediation: effective sunlight driven degradation of organic dyes and rapid heavy metal adsorption. Chem Eng J 325:588–600. https://doi.org/10.1016/j.cej.2017.05.105

Richardson SD, Ternes TA (2018) Water analysis: emerging contaminants and current issues. Anal Chem 90:398–428. https://doi.org/10.1021/acs.analchem.7b04577

Samadi M, Zirak M, Naseri A et al (2016) Recent progress on doped ZnO nanostructures for visible-light photocatalysis. Thin Solid Films 605:2–19. https://doi.org/10.1016/j.tsf.2015.12.064

Senthilraja A, Krishnakumar B, Nawabjan SA et al (2016) Facile synthesis of Y2S3/ZnO nanocomposite and its catalytic performance in the degradation of methylene blue using UV-A/solar illumination. J Water Process Eng 12:32–40. https://doi.org/10.1016/j.jwpe.2016.06.002

Smith AR, John G (2016) Azo dye toxicity : a measure of toxic effect metabolized azo dyes have on the body. 1–4

Song S, Ma Y, Shen H et al (2015) Removal and recycling of ppm levels of methylene blue from an aqueous solution with graphene oxide. RSC Adv 5:27922–27932. https://doi.org/10.1039/c4ra16982d

Stanley R, Jebasingh JA, Manisha Vidyavathy S (2019) Enhanced sunlight photocatalytic degradation of methylene blue by rod-like ZnO-SiO2 nanocomposite. Optik (stuttg) 180:134–143. https://doi.org/10.1016/j.ijleo.2018.11.084

Stanley R, Jebasingh JA, Vidyavathy SM et al (2021) Excellent photocatalytic degradation of methylene blue, rhodamine B and methyl orange dyes by Ag-ZnO nanocomposite under natural sunlight irradiation. Optik (stuttg) 231:166518. https://doi.org/10.1016/j.ijleo.2021.166518

Sun JH, Dong SY, Feng JL et al (2011) Enhanced sunlight photocatalytic performance of Sn-doped ZnO for Methylene Blue degradation. J Mol Catal A Chem 335:145–150. https://doi.org/10.1016/j.molcata.2010.11.026

Wang X, Wan X, Xu X, Chen X (2014) Facile fabrication of highly efficient AgI/ZnO heterojunction and its application of methylene blue and rhodamine B solutions degradation under natural sunlight. Appl Surf Sci 321:10–18. https://doi.org/10.1016/j.apsusc.2014.09.103

Welderfael T, Pattabi M, Pattabi RM, Arun Kumar Thilipan G (2016) Photocatalytic activity of Ag-N co-doped ZnO nanorods under visible and solar light irradiations for MB degradation. J Water Process Eng 14:117–123. https://doi.org/10.1016/j.jwpe.2016.11.001

World Health Organization International Agency for Research on Cancer (2015) Methylene blue monograph. 108

Yang J, Li X, Sun D et al (2014) Direct sunlight responsive Ag–ZnO heterostructure photocatalyst: enhanced degradation of rhodamine B. J Phys Chem Solids 78:35–40. https://doi.org/10.1016/j.jpcs.2014.11.004

Yu X, Wei P, Li Y (2019) Enhanced sunlight photocatalytic performance of ZnO/ZnS binary heterostructure sheets. Mater Lett 240:284–286. https://doi.org/10.1016/j.matlet.2018.12.136

Authors and Affiliations

R. Stanley[1,3] · J. Alphas Jebasingh[2] · S. Manisha Vidyavathy[3]

✉ J. Alphas Jebasingh
alphas.james@gmail.com

[1] Department of Chemical Engineering, Malaviya National Institute of Technology (MNIT), Jaipur 302017, India

[2] Department of Electronics and Communication Ensgineering, Muthayammal Engineering College, Namakkal 637408, India

[3] Department of Ceramic Technology, Anna University, Chennai 600025, India